



# Glutamate-activated BK channel complexes formed with NMDA receptors

Jiyuan Zhang<sup>a,1</sup>, Xin Guan<sup>a,1</sup>, Qin Li<sup>a,2</sup>, Andrea L. Meredith<sup>b</sup>, Hui-Lin Pan<sup>a</sup>, and Jiusheng Yan<sup>a,3</sup>

<sup>a</sup>Department of Anesthesiology and Perioperative Medicine, The University of Texas MD Anderson Cancer Center, Houston, TX 77030; and <sup>b</sup>Department of Physiology, The University of Maryland School of Medicine, Baltimore, MD 20201

Edited by Fred J. Sigworth, Yale University, New Haven, CT, and approved August 10, 2018 (received for review February 11, 2018)

**The large-conductance calcium- and voltage-activated K<sup>+</sup> (BK) channel has a requirement of high intracellular free Ca<sup>2+</sup> concentrations for its activation in neurons under physiological conditions. The Ca<sup>2+</sup> sources for BK channel activation are not well understood. In this study, we showed by coimmunopurification and colocalization analyses that BK channels form complexes with NMDA receptors (NMDARs) in both rodent brains and a heterologous expression system. The BK–NMDAR complexes are broadly present in different brain regions. The complex formation occurs between the obligatory BK $\alpha$  and GluN1 subunits likely via a direct physical interaction of the former's intracellular S0–S1 loop with the latter's cytosolic regions. By patch-clamp recording on mouse brain slices, we observed BK channel activation by NMDAR-mediated Ca<sup>2+</sup> influx in dentate gyrus granule cells. BK channels modulate excitatory synaptic transmission via functional coupling with NMDARs at postsynaptic sites of medial perforant path-dentate gyrus granule cell synapses. A synthesized peptide of the BK $\alpha$  S0–S1 loop region, when loaded intracellularly via recording pipette, abolished the NMDAR-mediated BK channel activation and effect on synaptic transmission. These findings reveal the broad expression of the BK–NMDAR complexes in brain, the potential mechanism underlying the complex formation, and the NMDAR-mediated activation and function of postsynaptic BK channels in neurons.**

BK channel | NMDA receptor | dentate gyrus granule cells | synaptic transmission | protein interactions

**T**he large-conductance calcium- and voltage-activated K<sup>+</sup> (BK) channel is a unique member of the K<sup>+</sup> channel family characterized by exceptionally large single-channel conductance and dual regulation of its activity by two independent physiological signals: membrane voltage and intracellular free Ca<sup>2+</sup> ([Ca<sup>2+</sup>]<sub>i</sub>). Upon activation by elevation of [Ca<sup>2+</sup>]<sub>i</sub> levels, BK channels can generate large single-channel K<sup>+</sup> efflux and, consequently, rapid membrane repolarization, which can limit further Ca<sup>2+</sup> flux through membrane depolarization-activated Ca<sup>2+</sup> channels. Via this negative-feedback mechanism, BK channel-mediated K<sup>+</sup> signaling plays a powerful integrative role in regulating cellular excitability and calcium signaling in electrically excitable cells (1, 2). BK channels are critically involved in various cellular and physiological processes. In central neurons, BK channels regulate neuronal firing and neurotransmitter release (3–5) and are involved in motor coordination (6), rhythmic control of the circadian clock (7), and frequency tuning of cochlear hair cells (8). Mutation or dysregulation of neuronal BK channels can cause epilepsy and paroxysmal dyskinesia (9, 10). BK channels also control the contractile tone of smooth muscle and are involved in the regulation of vascular blood pressure (11), the urinary bladder (12), and erectile function (13). In nonexcitable secretory epithelial cells, BK channels provide an essential pathway for resting K<sup>+</sup> efflux (14).

A BK channel is a homotetrameric channel consisting of four identical subunits of its pore-forming Ca<sup>2+</sup>- and voltage-sensing  $\alpha$  subunit (BK $\alpha$ ; encoded by the *KCNMA1* gene) (*SI Appendix, Fig. S1A*) either alone or in association with its regulatory  $\beta$  or  $\gamma$  subunit (15). BK channels belong to the family of Ca<sup>2+</sup>-activated

K<sup>+</sup> channels that also includes the intermediate-conductance K<sup>+</sup> (IK) and the small-conductance K<sup>+</sup> (SK) channels. BK channels are generally considered to be high-threshold channels for activation by voltage and Ca<sup>2+</sup> except in the presence of the non-neuronal auxiliary  $\gamma$ 1 and  $\gamma$ 2 subunits (16, 17). Within the physiological range of membrane voltages (less than or equal to +40 mV), the required [Ca<sup>2+</sup>]<sub>i</sub> concentration for significant BK channel activation [e.g., half-maximal effective concentration (EC<sub>50</sub>) > 10  $\mu$ M at 30 mV (18)] is generally much higher than the cellular global [Ca<sup>2+</sup>]<sub>i</sub> level at resting (less than or equal to  $\sim$ 0.1  $\mu$ M) and excited (less than or equal to  $\sim$ 1  $\mu$ M) states (*SI Appendix, Fig. S1B*). Therefore, native BK channels must localize with Ca<sup>2+</sup> sources within a nanodomain (i.e., a conceptual region within a few tens of nanometers from the cytoplasmic mouth of a Ca<sup>2+</sup> channel) (19, 20) to be physiologically active and functional (21) (*SI Appendix, Fig. S1C*). In contrast with BK channels, IK and SK channels have high affinity for Ca<sup>2+</sup> (EC<sub>50</sub>  $\sim$  0.3–0.5  $\mu$ M), which theoretically relieves them from the requirement of close interaction with Ca<sup>2+</sup> sources for functional coupling, even in the presence of the Ca<sup>2+</sup> chelator ethylene glycol-bis( $\beta$ -aminoethyl ether)-*N,N,N',N'*-tetraacetic acid (EGTA) (22). Despite a lack of evidence of physical association of SK channels with Ca<sup>2+</sup> channels, SK channels were found to be functionally coupled with Ca<sup>2+</sup> channels such as L-type CaV channels and

## Significance

**Large-conductance BK channels are dually activated by voltage and Ca<sup>2+</sup> and play a powerful integrative role in regulating cellular excitability and Ca<sup>2+</sup> signaling in neurons. However, BK channels have a requirement of high intracellular free Ca<sup>2+</sup> concentrations for activation under physiological conditions, and the Ca<sup>2+</sup> sources for their activation are not well understood. In this work, we establish that BK channels physically form protein complexes with Ca<sup>2+</sup>-permeable NMDA receptors via their obligatory BK $\alpha$  and GluN1 subunits. The activation mechanism and function of postsynaptic BK channels at synapses remain largely unknown. We found that postsynaptic BK channels in medial perforant path-dentate gyrus granule cell synapses are activated by NMDA receptor-mediated Ca<sup>2+</sup> influx and modulate excitatory synaptic transmission.**

Author contributions: J.Z., X.G., Q.L., H.-L.P., and J.Y. designed research; J.Z., X.G., Q.L., and J.Y. performed research; A.L.M. contributed new reagents/analytic tools; J.Z., X.G., Q.L., and J.Y. analyzed data; and J.Z., X.G., Q.L., and J.Y. wrote the paper.

The authors declare no conflict of interest.

This article is a PNAS Direct Submission.

Published under the PNAS license.

<sup>1</sup>J.Z. and X.G. contributed equally to this work.

<sup>2</sup>Present address: Department of Urology, Zhongnan Hospital of Wuhan University, Wuhan 430071, China.

<sup>3</sup>To whom correspondence should be addressed. Email: JYan1@mdanderson.org.

This article contains supporting information online at [www.pnas.org/lookup/suppl/doi:10.1073/pnas.1802567115/-DCSupplemental](http://www.pnas.org/lookup/suppl/doi:10.1073/pnas.1802567115/-DCSupplemental).

Published online September 4, 2018.

*N*-methyl-D-aspartate receptors (NMDARs) in hippocampal CA1 neurons (23–25).

In  $\text{Ca}^{2+}$  signaling, short coupling distances between  $\text{Ca}^{2+}$  sensors and  $\text{Ca}^{2+}$ -permeable channels within nanodomains can produce high efficacy, speed, and energy efficiency in  $\text{Ca}^{2+}$  signaling (19, 20). This is demonstrated by the relatively well-established coupling of BK channels with the voltage-gated  $\text{Ca}^{2+}$  (CaV) channels (21). BK channels were found to be physically associated with CaV1.2 and CaV2.1 channels in brain tissue and heterologous expression systems (21) and activated by  $\text{Ca}^{2+}$  influx through these channels in the presence of EGTA in heterologous expression systems (21, 26), native chromaffin cells (21, 27), and neurons in brain slices (28–31). In an early 2001 study (32), BK channels were also found to be activated by NMDAR-mediated  $\text{Ca}^{2+}$ -influx at extrasynaptic sites in rat olfactory bulb granule cells, which conferred a novel neuronal activity-inhibitory role on NMDARs. Since then, however, the underlying molecular basis for BK–NMDAR coupling and the presence and function of BK–NMDAR coupling in any other brain regions, neurons, and subcellular locations remain fully unknown.

NMDARs are ligand- and voltage-gated  $\text{Ca}^{2+}$  permeable cation channels, the opening of which requires coincident neurotransmitter glutamate binding and membrane depolarization-induced release of pore blockade caused by extracellular  $\text{Mg}^{2+}$  (33). NMDARs are heterotetrameric glutamate-gated cation channels composed of two GluN1 subunits and two GluN2 (A–D) or GluN3 (A–B) subunits. BK channels and NMDARs are traditionally considered presynaptic and postsynaptic channels, respectively. In this study, we showed that BK channels are physically associated and colocalized with NMDARs in both the brain and heterologous expression system via interactions between their obligatory BK $\alpha$  and GluN1 subunits on the intracellular side. We further found that BK channels play a novel role in regulation of synaptic transmission via functional coupling with postsynaptic NMDARs in the dentate gyrus.

## Results

### BK Channels and NMDARs Form Protein Complexes in Rat Brains.

Using an immobilized rabbit polyclonal anti-GluN1 antibody, we performed immunopurification of NMDARs from membrane-enriched fractions of adult (9- to 10-wk-old) rat whole brains (Fig. 1A). We observed a major protein band at a size corresponding to that of GluN1 in a sample purified with the anti-GluN1 antibody, but not in negative control samples obtained with a nonspecific rabbit IgG (Fig. 1B). We analyzed immunopurified samples using nanoflow liquid chromatography tandem-mass spectrometry and identified GluN1 as one of the most abundant proteins in them. We also identified other NMDAR subunits (GluN2A, GluN2B, GluN2C, and GluN3A) that were absent from the negative control sample (*SI Appendix, Table S1*), suggesting that the integrity of NMDARs was largely retained in the affinity-purified sample. Of note, mass-spectrometric analysis also identified BK $\alpha$  in the affinity-purified NMDAR samples, but not in negative control samples (Fig. 1C). We confirmed the mass spectrometry results using immunoblot analysis, showing that BK $\alpha$  was detected by an anti-BK $\alpha$  antibody in a sample purified from rat brains with the anti-GluN1 antibody, but not in a control sample (Fig. 1D). We also performed immunopurification of BK channels using an anti-BK $\alpha$  antibody (Fig. 1A) and observed that GluN1 was present in a purified BK sample according to both mass spectrometry (Fig. 1E) and immunoblot analysis (Fig. 1F).

To confirm that BK channels are complexed with heteromeric functional NMDARs, we performed tandem immunopurification with an anti-BK $\alpha$  antibody in the first round and an anti-GluN1 antibody in the second round to specifically purify the protein complexes containing both BK $\alpha$  and GluN1 (Fig. 1A). Using immunoblot analysis, we found that both GluN2A and GluN2B were present in affinity-purified BK $\alpha$ –GluN1 complexes (Fig. 1G), suggesting that BK channels are indeed associated with

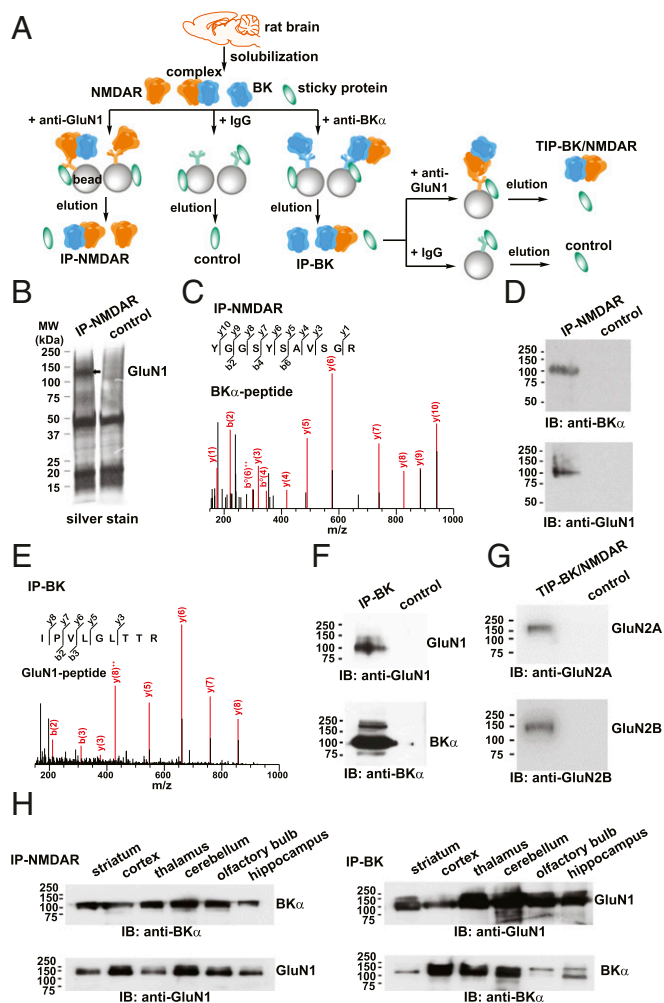


**Fig. 1.** BK channels and NMDARs form complexes in rat brains. (A) Schematic of the sample-preparation protocols for the immunopurified NMDAR (IP-NMDAR) and BK channel (IP-BK), tandem immunopurified BK–NMDAR complex (TIP-BK/NMDAR), and negative control samples. (B) SDS/PAGE and silver stain analysis of the IP-NMDAR and control samples. (C) Tandem mass spectrometric spectra of a unique peptide of BK $\alpha$  identified in the IP-NMDAR sample. (D) Immunoblot (IB) analysis of BK $\alpha$  and GluN1 in the IP-NMDAR sample. (E) Tandem mass spectrometric spectra of a unique peptide of GluN1 identified in the IP-BK sample. (F) Immunoblot analysis of GluN1 and BK $\alpha$  in the IP-BK sample. (G) Immunoblot analysis of GluN2A and GluN2B in the TIP-BK/NMDAR sample. (H) Immunoblot analysis of BK $\alpha$  and GluN1 in IP-NMDAR (Left) and IP-BK (Right) samples prepared from different brain regions.

heteromeric functional NMDARs in the rat brain. To determine whether the association between BK $\alpha$  and GluN1 is brain region-specific or broadly present in different brain regions, we performed immunopurification of BK channels and NMDARs in several brain regions. We observed that BK–NMDAR complexes were ubiquitously present, as the anti-GluN1 antibody could pull down BK channels and the anti-BK $\alpha$  antibody could pull down GluN1 in all examined brain regions, including the hippocampus, cerebellum, cortex, thalamus, striatum, and olfactory bulb (Fig. 1H).

### BK Channels and NMDARs Specifically Interact via Their Obligatory BK $\alpha$ and GluN1 Subunits.

To investigate the molecular basis for BK–NMDAR complex formation, we used a heterologous expression system with HEK-293 cells to manipulate protein expression without complications of endogenous BK channel

or NMDAR expression. We coexpressed BK $\alpha$  with GluN1, GluN2A, and GluN2B in HEK-293 cells and performed immunoprecipitation and immunoblot analysis. We observed that in the absence of GluN2A or GluN2B expression, the anti-BK $\alpha$  antibody could effectively pull down GluN1 together with BK $\alpha$  and, similarly, that an anti-FLAG antibody could effectively pull down BK $\alpha$  together with FLAG-tagged GluN1 (Fig. 2A). However, GluN2A and GluN2B were pulled down together with BK $\alpha$  only in the presence of GluN1 expression (Fig. 2B and C). Although GluN2A and GluN2B may not be expressed on the plasma membrane in the absence of GluN1, they should still be able to be pulled down together with BK $\alpha$  if they can interact with BK $\alpha$  on intracellular membranes such as the endoplasmic reticulum, where most membrane proteins might accumulate when overexpressed in HEK-293 cells. These results indicated that BK $\alpha$  interacts with the NMDARs' obligatory GluN1 subunit in a regulatory subunit-independent manner. To determine the specificity of the BK–NMDAR interactions, we analyzed the association of BK channels with the other two classes of ionotropic glutamate receptors. We found that the GluK1 and GluK2 subunits of kainate receptors and GluR1 and GluR2 subunits of AMPA receptors did not interact with BK $\alpha$  when they were coexpressed in HEK-293 cells (*SI Appendix, Fig. S24*). Similarly, GluR1 and GluR2 were absent from BK channel samples affinity-purified from rat brains (*SI Appendix, Fig. S2B*).

To identify the protein regions involved in BK–NMDAR interactions, we generated truncation mutants of BK $\alpha$  and GluN1 and used chimeric constructs of GluN1. We observed that the anti-FLAG antibody, which recognized FLAG-tagged GluN1, can pull down the BK $\alpha$  N-terminal region (residues 1–324), but not cytoplasmic C-terminal region (residues 325–1113), although the latter had much higher expression than did the former (*SI Appendix, Fig. S3A*). The BK $\alpha$  N-terminal region contains a long

intracellular S0–S1 loop region, which may participate in protein–protein interactions because of its lengthy and flexible feature as its structure is disordered in cryo-EM structures of *Aplysia* BK channels (34, 35). Upon deletion of the residues 46–93 in the S0–S1 loop region, we found that the resulting BK $\alpha$   $\Delta$ 46–93 mutant became largely defective in its association with GluN1, as both anti-BK $\alpha$  and -GluN1 antibodies can barely pull down the other partners (Fig. 2D). To determine whether the S0–S1 loop region is directly involved in the BK $\alpha$ –GluN1 interaction, we included a synthesized peptide of the S0–S1 loop region (residues 46–93) during the immunoprecipitation procedure. We observed that the S0–S1 loop peptide greatly reduced the amount of BK $\alpha$  that was coimmunoprecipitated with GluN1, while the scrambled control peptide had little effect (Fig. 2E), suggesting that the S0–S1 loop peptide can compete with BK $\alpha$  in their interactions with GluN1.

Using GluN1 truncation mutants, we observed that the GluN1 C-terminal region (residues 560–938) was much more effective than its extracellular N-terminal region (residues 1–559) in their coimmunoprecipitation with BK $\alpha$ , although the latter expressed much better than did the former (*SI Appendix, Fig. S3B*). To maintain the structural integrity of GluN1, we used its chimeric mutants that were previously created with GluK2 and demonstrated to be functional in forming glutamate receptors (36, 37). Similar to those observed with the GluN1 truncation mutants, we observed that the chimeric construct N1/K2<sup>C</sup>, in which the GluN1's C-terminal part (the TM domain and intracellular C terminus) was replaced with that of GluK2 (*SI Appendix, Fig. S3C*), was markedly decreased in its coimmunoprecipitation with BK $\alpha$  (Fig. 2F). We further observed that the GluN1's TM domain, including connecting loops, might be involved in interactions with BK $\alpha$  as a significant decrease in the association of GluN1 with BK $\alpha$  also occurred when the former's TM domain was replaced with that of GluK2 (*SI Appendix, Fig. S3C and D*).

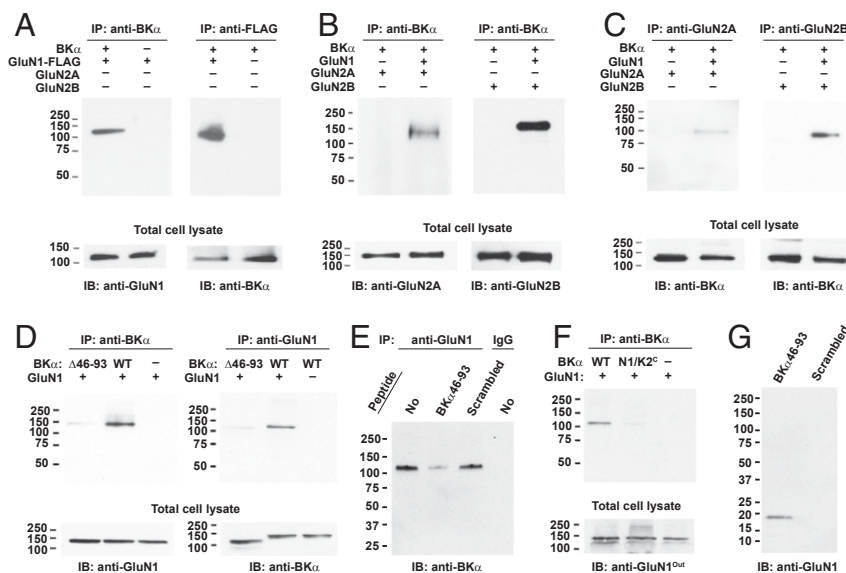


**Fig. 2.** BK channels and NMDARs interact via BK $\alpha$  and GluN1 in HEK-293 cells. (A) Reciprocal pull-down of GluN1 and BK $\alpha$  by anti-BK $\alpha$  and -GluN1 antibodies in the absence of expression of any other NMDAR subunit. IB, immunoblot; IP, immunoprecipitation. (B) Pull-down of GluN2A and GluN2B by an anti-BK $\alpha$  antibody only in the presence of GluN1 expression. (C) Pull-down of BK $\alpha$  by an anti-GluN2A or -GluN2B antibody only in the presence of GluN1 expression. (D) Reciprocal pull-down assay showed that the BK $\alpha$  was largely defective in its association with GluN1 upon deletion of its S0–S1 loop region (residues 46–93). (E) Pull-down of BK $\alpha$  by an anti-GluN1 was interfered by a synthesized peptide of the BK $\alpha$ 's S0–S1 loop region (residues 46–93), but not by a scrambled peptide. The peptides were added at a concentration of 1 mg/ml to cell lysates that were equally divided from the same lysate of cells coexpressing BK $\alpha$  and GluN1. (F) Pull-down of GluN1 by an anti-BK $\alpha$  antibody showed that the BK $\alpha$ –GluN1 association was markedly decreased with the GluN1 N1/K2<sup>C</sup> mutant in which the C-terminal part, including TM domain (residues 527–647 and 781–826) and C-terminal domain (residues 827–920), was replaced by those of GluK2. (G) Pull-down of the GluN1's cytosolic regions by the BK $\alpha$ 46–93 peptide, but not by the scrambled peptide. The peptides were biotinylated on their N termini and immobilized on streptavidin agarose. The fusion construct of the GluN1's cytosolic regions (residues 563–587 and 813–920) was 6 $\times$  His-tagged in its C terminus, expressed in *E. coli*, and purified with IMAC chromatography.

To determine whether the BK $\alpha$ 's cytosolic S0–S1 loop region can directly interact with the GluN1's cytosolic regions, we expressed a 6 $\times$  His-tagged fusion protein of the GluN1's cytosolic regions (residues 563–587 for the M1–M2 loop region and residues 813–920 for the C terminus) in *Escherichia coli* and purified it with immobilized metal affinity chromatography (IMAC). We found that the purified fusion protein of the GluN1's cytosolic regions was precipitated by the biotinylated S0–S1 loop peptide immobilized on Strep-Tactin agarose beads, but not by the scrambled peptide (Fig. 2G). These results suggest that BK $\alpha$  and GluN1 can directly interact with each other via their cytosolic regions.

**BK $\alpha$  and GluN1 Colocalize in HEK-293 Cells and Mouse Brains.** In situ proximity ligation assay (PLA) is an established method of visualizing protein–protein interactions in cells (38). This assay combines antibody-based protein recognition and nucleotide-based rolling circle amplification to allow a protein complex to be fluorescently labeled only when the two epitopes on the interacting proteins are in close proximity (SI Appendix, Fig. S4A). To probe the surface expression of the BK $\alpha$ –GluN1 complexes, we introduced the V5- and FLAG-tags on extracellular N termini of BK $\alpha$  and GluN1, respectively. Upon coexpression of the V5-BK $\alpha$  and FLAG-GluN1, in situ PLA with anti-V5 and -FLAG antibodies under a cell-nonpermeabilized condition produced PLA signals that outline the perimeters of HEK-293 cells (Fig. 3A), suggesting that the BK $\alpha$ –GluN1 complexes were expressed on plasma membranes. Under a cell-permeabilized condition, we observed that coexpression of GluN1 with full-length BK $\alpha$  or the N-terminal part of BK $\alpha$  produced strong PLA signals, while coexpression of GluN1 with the C-terminal part of BK $\alpha$  produced much weaker PLA signals (SI Appendix, Fig. S4B), confirming that

the PLA signals of BK $\alpha$ –GluN1 complexes were produced by physical association between these two proteins.

To examine colocalization of endogenously expressed BK channels and NMDARs with in situ PLA, we examined the antigen specificities of a mouse monoclonal anti-BK $\alpha$  antibody (L6/60; NeuroMab) and a rabbit monoclonal anti-GluN1 antibody (AB9864R; EMD Millipore). We observed that these two antibodies produced strong point-like PLA signals only when both BK $\alpha$  and GluN1 were expressed, validating the antigen specificities of these antibodies for in situ PLA (SI Appendix, Fig. S4C). We performed in situ PLA with these two antibodies on brain slices and found that the PLA signals were broadly present in different regions of the hippocampus. In the dentate gyrus of Nestin-Cre<sup>-</sup>/KCNMA1<sup>fl/fl</sup> mice in which BK $\alpha$  expression remained intact, PLA signals of the BK $\alpha$ –GluN1 complexes were most abundant in the molecular-layer region (Fig. 3B), which is consistent with the predominant dendritic distribution of NMDARs. PLA signals were barely detectable in brain slices from Nestin-Cre<sup>+</sup>/KCNMA1<sup>fl/fl</sup> mice in which tissue-specific BK $\alpha$ -knockout (KO) occurred in neurons (39) (Fig. 3C). Similarly, immunofluorescent labeling of BK $\alpha$  and GluN1 demonstrated an overlap in staining of the dentate gyrus in Nestin-Cre<sup>-</sup>/KCNMA1<sup>fl/fl</sup> mice, whereas the immunostaining signal of the anti-BK $\alpha$  antibody was much weaker in the Nestin-Cre<sup>+</sup>/KCNMA1<sup>fl/fl</sup> BK $\alpha$ -KO mice (SI Appendix, Fig. S5). These results thus demonstrate that BK channels and NMDARs can colocalize under conditions of both heterologous expression in HEK-293 cells and endogenous expression in the brain.

**NMDAR-Mediated Ca<sup>2+</sup> Influx Activates BK Channels in Dentate Gyrus Granule Cells.** We performed whole-cell voltage-clamp recording of mature dentate gyrus granule cells in the presence of the intracellular Ca<sup>2+</sup> chelator EGTA. Using acute adult mouse brain slices, we applied glutamate and glycine close to the cell bodies of mature granule cells using a puffer pipette. At more negative voltages, we mainly observed the inward currents of NMDARs. However, as the applied voltages became less negative, a prominent outward current developed (Fig. 4A). The glutamate-induced outward currents were fully abolished in the presence of paxilline, which is a BK channel pore blocker (40) (Fig. 4B and C), but only partially reduced in the presence of the BK channel inhibitor iberiotoxin (IbTX) (SI Appendix, Fig. S6), which agreed with the presence of the IbTX-resistant BK $\alpha$ / $\beta$ 4 channel in the dentate gyrus (10). Upon perfusion of the NMDAR antagonist (2R)-amino-5-phosphonovaleric acid (AP5), the glutamate-induced BK channel outward currents were largely diminished (Fig. 4B and C), indicating the involvement of NMDARs in glutamate-induced BK channel activation. Application of the NMDAR pore blocker MK-801 to bath solution also led to suppression of the glutamate-induced outward BK channel currents (SI Appendix, Fig. S6), indicating involvement of the ion-conducting function, but not the ion influx-independent metabolic function of NMDARs (41, 42).

When a BK channel is within a short distance from an NMDAR (e.g.,  $\leq 30$  Å), we predicted from calculation (SI Appendix, Fig. S1C) that the availability of free Ca<sup>2+</sup> ions originating from NMDAR activity would be largely retained in the presence of EGTA and significantly reduced, but not fully abolished, by the fast Ca<sup>2+</sup> chelator 1,2-bis(*o*-aminophenoxy) ethane-*N,N,N',N'*-tetraacetic acid (BAPTA). We found that the amplitudes of glutamate-induced outward currents of BK channels were similar when granule cells were loaded intracellularly with 0.2 and 2 mM EGTA and became significantly smaller, but not fully lost, when the cells were loaded with 2 mM BAPTA (Fig. 4B and C). These results demonstrate that BK channels in hippocampal dentate granule cells are potently activated by NMDAR-mediated Ca<sup>2+</sup> influx within a short coupling distance. To determine whether the BK $\alpha$ –GluN1 physical interactions are

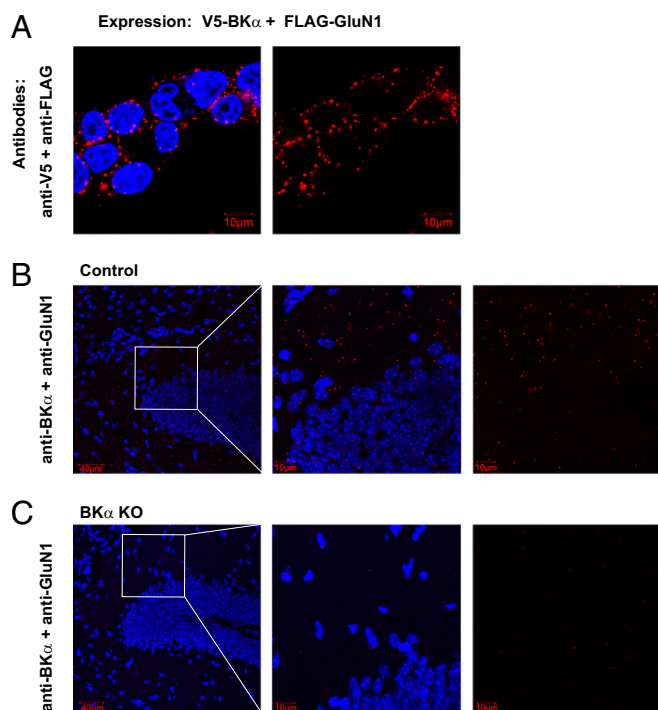


**Fig. 3.** In situ PLA of BK $\alpha$  and GluN1 colocalization in HEK-293 cells and mouse brains. (A) PLA signals (red dots) probed with anti-V5 and -FLAG antibodies under a nonpermeabilized condition were detected in HEK-293 cells coexpressing V5-BK $\alpha$  and FLAG-GluN1. (B and C) In situ PLA of BK $\alpha$ –GluN1 complexes in the hippocampal dentate gyrus of control (Nestin-Cre<sup>-</sup>/KCNMA1<sup>fl/fl</sup>) mice (B) and neuron-specific BK $\alpha$  KO (Nestin-Cre<sup>+</sup>/KCNMA1<sup>fl/fl</sup>) mice (C). Nuclei are shown in blue (DAPI). (Scale bars: 40 or 10  $\mu$ m.)

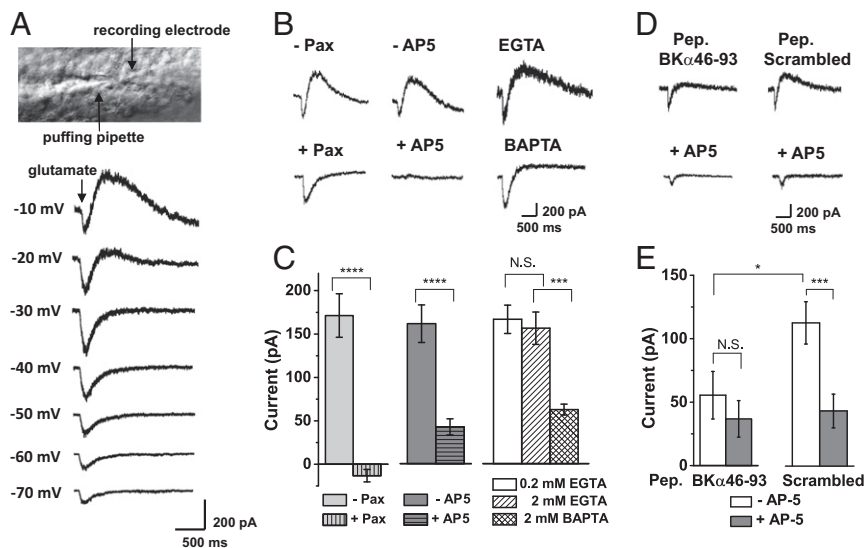


**Fig. 4.** Glutamate-induced BK channel activation via NMDARs in mature dentate gyrus granule cells. (A) Whole-cell recording of glutamate-induced currents at different holding membrane voltages upon somatic puff application of 100  $\mu$ M glutamate and 10  $\mu$ M glycine for 100 ms. (B) Representative glutamate-induced currents at  $-10$  mV in the absence and presence of the BK channel blocker paxilline (Pax; 10  $\mu$ M) and NMDAR antagonist AP5 (200  $\mu$ M) and in the presence of the intracellular chelators EGTA and BAPTA. (C) Averaged effects of paxilline ( $n = 13$ ), AP5 ( $n = 13$ ), and intracellular chelators (0.2 mM EGTA,  $n = 26$ ; 2 mM EGTA,  $n = 8$ ; 2 mM BAPTA,  $n = 8$ ) on the glutamate-induced outward currents. (D) Representative glutamate-induced currents at  $-10$  mV with recording pipette solution containing 0.5 mg/mL BK $\alpha$ 46–93 peptide or scrambled peptide and the bath solution perfused with/without AP5 (200  $\mu$ M). Pep., peptide. (E) Averaged amplitudes of glutamate-induced outward currents in the presence of the intracellularly loaded BK $\alpha$ 46–93 ( $n = 9$ ) or scrambled ( $n = 8$ ) peptide. The current amplitudes were calculated from the peak amplitudes of outward currents relative to the current levels before drug application. Data are shown as means  $\pm$  SEM. Statistical differences were evaluated using a *t* test. N.S., not significant. \* $P < 0.05$ ; \*\*\* $P < 0.001$ ; \*\*\*\* $P < 0.0001$ .

involved in the NMDAR-mediated BK channel activation, we loaded the granule cells intracellularly with the synthesized peptide of the BK $\alpha$ 's S0–S1 loop region via recording pipettes. We found that the intracellular application of the S0–S1 loop peptide (0.5 mg/mL) caused a great reduction in the amplitudes of glutamate-induced outward BK channel currents compared with those observed in the presence of the scrambled peptide (Fig. 4 D and E), suggesting that physical interactions are involved for the functional coupling of BK channels with NMDARs.

To determine whether functional coupling of BK channels with NMDARs also occurs in the simpler heterologous expression system, we performed whole-cell patch-clamp recording of NMDA-evoked NMDAR currents and the concomitant BK channel currents in the presence of 5 mM EGTA in HEK-293 cells expressing BK $\alpha$ , GluN1, and GluN2A. Similar to the endogenous BK–NMDAR coupling in dentate granule cells described above, extracellular perfusion of the NMDAR agonist NMDA onto the HEK-293 cell body induced BK channel outward currents at negative voltages (e.g.,  $-20$  mV), and these currents were eliminated in the presence of AP5 or IbTX (SI Appendix, Fig. S7A). In excised inside-out membrane patches of HEK-293 cells, we observed that the events of channel opening for both NMDARs and BK channels at a negative membrane voltage (e.g.,  $-40$  mV) were markedly increased at the single-channel level upon flash photolysis of caged NMDA in the pipette electrode solution (SI Appendix, Fig. S7 B and C). Our electrophysiological data thus demonstrated EGTA-insensitive functional coupling of BK channels with NMDARs in HEK-293 cells.

**BK Channels Regulate Synaptic Transmission via Structural and Functional Coupling with Postsynaptic NMDARs at Synapses in Dentate Gyrus Granule Cells.** To determine whether BK–NMDAR coupling affects synaptic transmission, we measured the evoked excitatory postsynaptic potentials (EPSPs) of dentate gyrus granule cells in the presence of intracellular EGTA upon stimulation of presynaptic fibers from the

medial perforant path (MPP) in the middle of the molecular layer (SI Appendix, Fig. S8). We observed that blockade of BK channels by extracellularly applied paxilline considerably increased the amplitude of evoked EPSPs to  $123 \pm 4\%$  of that recorded before the drug application (control) and that subsequent application of AP5 together with paxilline restored the amplitude of evoked EPSPs to  $96 \pm 6\%$  of that of the control (Fig. 5A). As expected for the opposite effects of the BK channel's outward  $K^+$  currents and the NMDARs' inward cation currents on membrane potentials, these data suggest that BK channel activity suppresses the EPSP amplitude, whereas NMDAR activity alone in the absence of BK channel activity potentiated the EPSP amplitude under the experimental conditions. Interestingly, we found that application of AP5 alone did not significantly affect the evoked EPSPs, whose amplitude remained at  $94 \pm 6\%$  of the control (Fig. 5B); this was similar to the combined effect of AP5 and paxilline on the evoked EPSPs (Fig. 5A). Further application of paxilline together with AP5 led to a decrease rather than an increase in the amplitude of evoked EPSPs (Fig. 5B). In the absence of paxilline, AP5 alone also caused a similar time-dependent decrease in the amplitude of evoked EPSPs (Fig. 5B), suggesting that paxilline does not affect synaptic transmission when NMDARs were inactive. The time-dependent effects of AP5 may be related to the metabotropic function of NMDARs (41, 42). To confirm that the observed paxilline-induced increase in the amplitude of EPSPs was caused by blockade of BK channels, we repeated the experiments using brain slices obtained from Nestin-Cre<sup>+</sup>/KCNMA1<sup>fl/fl</sup> BK $\alpha$ -KO mice. As we expected given the results described above, we found that in the absence of functional BK $\alpha$  expression, bath-applied paxilline had no effect on the amplitude of evoked EPSPs, whereas application of AP5 decreased the amplitude of evoked EPSPs by  $20 \pm 7\%$  (Fig. 5C). These results suggest that BK channel activity negatively regulates synaptic transmission and that such BK channel activity is induced by  $Ca^{2+}$  influx through NMDARs.

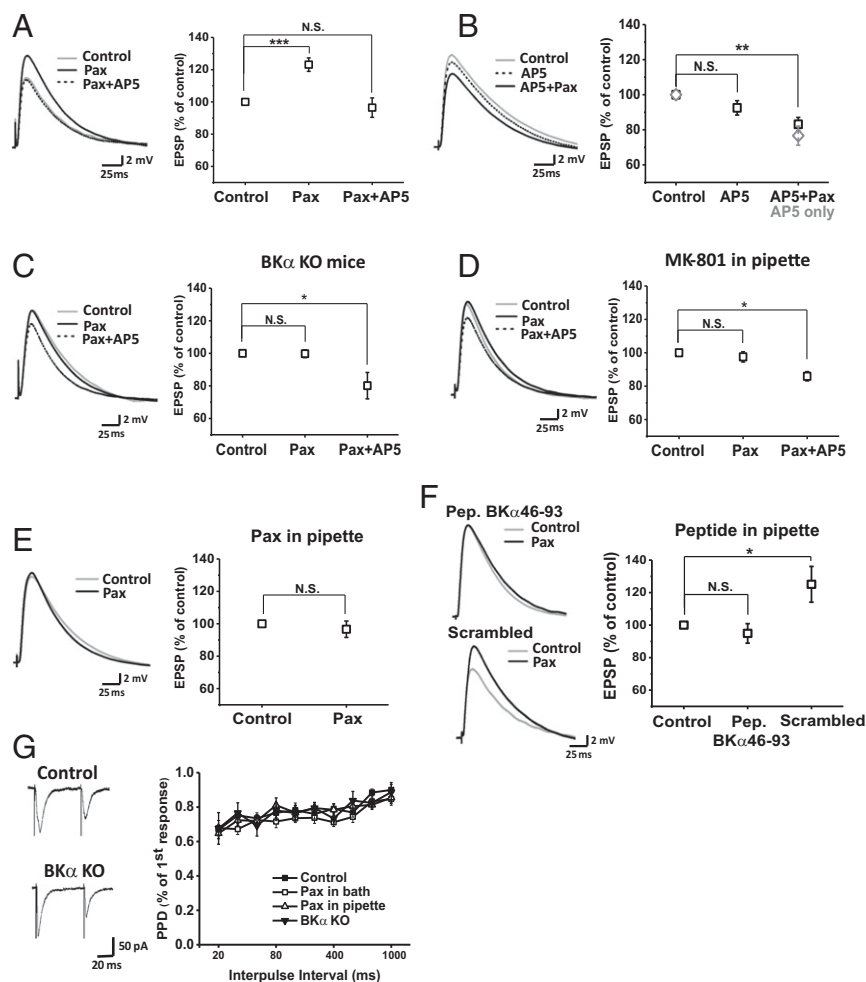


**Fig. 5.** Postsynaptic BK channels regulate synaptic transmission in mature dentate granule cells via NMDAR-mediated channel activation. (A) Effects of paxilline (Pax) alone and combined with AP5 on the amplitudes of evoked EPSPs ( $n = 13$ ). (B) Effects of AP5 alone and combined with paxilline on the amplitudes of evoked EPSPs ( $n = 13$ ). For comparison, the effects of AP5 alone on evoked EPSPs over a similar extended time course ( $n = 6$ ) were included in the averaged plot. (C) Effects of paxilline alone and combined with AP5 on the amplitudes of evoked EPSPs in mature granule cells in BK $\alpha$ -KO (Nestin-Cre<sup>+</sup>/KCNMA1<sup>fl/fl</sup>) mice ( $n = 9$ ). (D) The effect of paxilline alone (bath) and combined with AP5 (bath) on evoked EPSPs in the presence of intracellularly applied MK-801 ( $n = 9$ ). (E) Effects of paxilline on evoked EPSPs in the presence of intracellularly applied paxilline ( $n = 8$ ). (F) Effects of paxilline on evoked EPSPs in the presence of intracellularly applied 0.5 mg/mL BK $\alpha$ 46–93 ( $n = 8$ ) or scrambled ( $n = 7$ ) peptide. Pep., peptide. (G) Effects of extracellularly and intracellularly applied paxilline ( $n = 9$  and 7, respectively) and KO of BK channels (Nestin-Cre<sup>+</sup>/KCNMA1<sup>fl/fl</sup>) ( $n = 5$ ) on paired-pulse ratios. All experiments were done with regular C57BL/6 mice except as specified. Control, data obtained without or before drug application. Paxilline and AP5 were perfused in the bath solution at a concentration of 10 and 200  $\mu$ M, respectively, and they were applied either individually or combined together at a later stage of the experiment. Statistical differences were evaluated by using a  $t$  test. N.S., not significant. \* $P < 0.05$ ; \*\* $P < 0.01$ ; \*\*\* $P < 0.001$ .

Given that NMDAR activation at extrasynaptic sites requires significant glutamate spillover resulting from a series of repetitive synaptic activities (32), we expect that only NMDARs at synapses can be activated by glutamate released from presynaptic terminals in single pulse-evoked synaptic transmission experiments described above. We observed that intracellular application of MK-801 to dentate granule cells via recording pipettes fully suppressed paxilline's effect on the amplitude of EPSPs (Fig. 5D). Given that MK-801 is a channel pore blocker (43) whose intracellular application was commonly used to block NMDARs specifically in the recorded cells (44, 45), this result suggests that postsynaptic NMDARs at synapses are required for BK channels' effects on EPSPs. To confirm that postsynaptic BK channels were involved in regulation of the amplitude of EPSPs, we loaded the dentate granule cells with paxilline, which can also effectively block BK channels when applied intracellularly (40), via recording pipettes and found that further application of paxilline in a bath solution had little effect on the amplitude of

evoked EPSPs (Fig. 5E). Thus, the paxilline's potentiating effect on evoked EPSPs is caused by blocking postsynaptic BK channels that are activated by postsynaptic NMDAR-mediated Ca<sup>2+</sup> influx. To evaluate whether the physical interactions between BK channels and NMDARs are involved in the postsynaptic functional coupling of BK channels with NMDARs, we included the synthesized peptide of the BK $\alpha$ 's S0–S1 loop region in the recording pipette solution. We observed that the S0–S1 loop peptide (0.5 mg/mL) abolished the paxilline's potentiating effect on evoked EPSPs, while the scrambled peptide did not (Fig. 5F). Overall, these findings indicate that BK channels negatively regulate synaptic transmission via BK–NMDAR interactions and functional coupling at the postsynaptic site of MPP-dentate granule cell synapses.

Because BK channels are known to regulate neurotransmitter release in the presynaptic terminal in some neurons (4, 46–48), we measured the paired-pulse ratio of the amplitudes of the first and second evoked EPSCs to determine whether BK channels

regulate synaptic transmission at MPP-dentate granule cell synapses via their effect on presynaptic transmitter release. Similar to previous reports (49, 50), we observed paired-pulse depression upon paired-pulse stimulation at the MPP (Fig. 5G). We found that paired-pulse depressions over a wide range of intervals were not significantly different between WT and BK $\alpha$ -KO mice or among WT mice in the presence and absence of paxilline applied in a bath or pipette solution (Fig. 5G). Given that the paired-pulse ratio reflects the neurotransmitter release probability of presynaptic neurons (51), these results suggest that BK channels are not involved in regulating presynaptic neurotransmitter release in the MPP-dentate granule cell synapses under our experimental conditions.

## Discussion

Both BK channels and NMDARs are ubiquitously expressed in the mammalian central and peripheral nervous systems. In this study, we found that BK channels were physically associated with NMDARs in brain tissue and HEK-293 cells, but did not interact with other examined ionotropic glutamate receptors which are largely Ca<sup>2+</sup>-impermeable. The physical association between BK channels and NMDARs required only their obligatory subunits (BK $\alpha$  and GluN1), involving the former's intracellular S0–S1 loop region and the latter's TM region and intracellular C-terminal domain. As detected by using *in situ* PLA, BK $\alpha$  and GluN1 colocalized in both HEK-293 cells and mouse brain slices. Activation of BK channels by NMDAR-mediated Ca<sup>2+</sup> influx remained robust in the presence of EGTA under both endogenous (dentate gyrus granule cells) and heterologous (HEK-293 cells) expression conditions. Our biochemical analyses demonstrate that BK–NMDAR complexes are present in all examined brain regions. Therefore, we conclude that neuronal BK channels can specifically coassemble with NMDARs via direct protein–protein interactions within nanodomains in different brain regions and neurons.

To determine how strongly BK channel activation is coupled with NMDAR opening, we intracellularly applied EGTA and the fast chelator BAPTA, which differ greatly in their Ca<sup>2+</sup>-binding rates but have comparable Ca<sup>2+</sup> affinities (19). If the distance between BK channels and NMDARs is large ( $\geq 50$  nm), EGTA can significantly reduce the local [Ca<sup>2+</sup>]<sub>i</sub> level to no more than 2  $\mu$ M (*SI Appendix, Fig. S1C*), which is barely able to activate BK channels within physiological ranges of membrane voltages (*SI Appendix, Fig. S1B*). If the distance between these two channels is short, a high local [Ca<sup>2+</sup>]<sub>i</sub> concentration (e.g.,  $\geq 10$   $\mu$ M if the distance is  $\leq 15$  nm) can be reached, even in the presence of EGTA, which allows BK channels to be significantly activated (e.g.,  $P_o = 0.15$  at  $-10$  mV at 10  $\mu$ M [Ca<sup>2+</sup>]<sub>i</sub>). Within such a short distance, only BAPTA will be able to capture Ca<sup>2+</sup> on its way from the Ca<sup>2+</sup> release pore to Ca<sup>2+</sup> sensors and thus significantly reduce the local [Ca<sup>2+</sup>]<sub>i</sub> concentration (e.g., a change from 10  $\mu$ M with EGTA to 3  $\mu$ M with BAPTA at a distance of 15 nm). We found that BAPTA, compared with EGTA, can partially reduce the glutamate-induced BK channel currents in dentate granule cell somata. Given a protein size of  $\sim 10$  nm (parallel to the membrane) for both channels, the Ca<sup>2+</sup> sensors of a BK channel can be very close to the NMDAR channel pore (up to 10–15 nm), which agrees with our observation of their physical association, colocalization, and functional coupling in both brain slices and the heterologous expression system.

We found that both GluN2A and GluN2B were present in the neuronal BK–NMDAR complexes. In the adult central nervous system, GluN2B is mainly expressed at extrasynaptic sites, whereas GluN2A-containing receptors are enriched at postsynaptic sites at synapses (33). Thus, BK–NMDAR complexes may exist both extrasynaptically and synaptically. At extrasynaptic sites, functional BK–NMDAR coupling can be induced by glutamate spillover during a series of repetitive synaptic ac-

tivities in olfactory bulb granule cells (32). At synaptic sites, BK channels are generally considered to be axonal channels and involved in regulation of neurotransmitter release at the opposite presynaptic sides of postsynaptic NMDARs. However, postsynaptic BK channels were reported to account for  $\sim 20\%$  and 50% of immunogold-labeled synaptic BK channels in the stratum radiatum and stratum oriens, respectively, in the rat hippocampus (52). The function of postsynaptic BK channels at synapses has long been largely unexplored. In the present study, we found that BK channels do not have a significant role in the regulation of presynaptic neurotransmitter release at perforant path–dentate granule cell synapses under basal conditions. This result is consistent with those observed in CA3–CA1 synapses of acute rat brain slices, in which regulation of neurotransmitter release by BK channels occurred only in the presence of a Kv channel blocker 4-aminopyridine (5), which can also directly potentiate the activity of CaV channels (53). Of note, our data suggest that BK channels modulate synaptic transmission at perforant path–dentate granule cell synapses via a novel mechanism of postsynaptic BK–NMDAR coupling at synapses, which can be easily activated by presynaptically released glutamate during synaptic transmission.

Dentate gyrus granule cells are the first checkpoint for cortical information entering the hippocampus, where learning and memory take place. Knockout of the BK channel  $\beta 4$  subunit, which is highly expressed in dentate gyrus, altered the intrinsic firing properties of granule cells and led to temporal lobe seizures of the hippocampus in mice (10). Our findings on NMDAR-mediated BK channel activation and the modulatory effect of postsynaptic BK–NMDAR coupling on EPSPs in dentate granule cells provide a molecular basis for understanding the role of BK channels in hippocampal learning and memory (54–57). Because BK–NMDAR complexes exist in all examined brain tissues and even in the heterologous expression system, functional coupling of these two channels must be broad in the nervous system, where both channels are widely coexpressed. Glutamate-induced BK channel activation can cause membrane repolarization and subsequently facilitate voltage-dependent blockade of NMDARs by extracellular Mg<sup>2+</sup>. This helps explain previous reports of the requirement of both NMDAR and BK channel activities in inhibiting opioid release in the spinal dorsal horn (58) and BK channel-mediated negative feedback on NMDAR-mediated dendritic spine Ca<sup>2+</sup> transients in cartwheel cells of the dorsal cochlear nucleus (59). Our findings thus provide a molecular basis for exploring and understanding the broad physiological and pathological functions of BK channels and NMDARs within a framework of Ca<sup>2+</sup>-mediated cross-talk between these two ion channels.

BK channels and NMDARs are both ligand- and voltage-dependent channels. BK–NMDAR coupling and BK–CaV coupling (21, 22) differ in their activation, kinetics, subcellular localization, and function. Compared with the purely voltage-driven activation of BK channels via CaV channels, neurotransmitter release is also required for triggering NMDAR-mediated BK channel activation. NMDARs can provide more sustained Ca<sup>2+</sup> sources for BK channel activation than can CaV channels because of the slow time course of NMDAR deactivation. The kinetically tight coupling of BK and CaV channels occurs at presynaptic active zones and is particularly suitable for regulating presynaptic Ca<sup>2+</sup> entry and neurotransmitter release (60). In contrast, as we found in dentate granule cells, BK–NMDAR coupling at postsynaptic terminals produces the neurotransmitter release-dependent K<sup>+</sup> signaling that can regulate synaptic transmission and, likely, plasticity, as well.

## Methods

**Animals.** Sprague–Dawley rats (9–10 wk old) were used for immunopurification and proteomic and immunoblot analysis of BK–NMDAR complexes.

C57BL6 mice were used for immunofluorescent labeling, in situ PLA, and electrophysiological analysis of BK–NMDAR complexes. Neuron-specific BK $\alpha$  KO and WT mice were F2 nestin-Cre<sup>+</sup>/KCNMA1<sup>fl/fl</sup> and Nestin-Cre<sup>-</sup>/KCNMA1<sup>fl/fl</sup> mice that carry homozygous floxed KCNMA1 allele (KCNMA1<sup>fl/fl</sup>) in the presence and absence of Cre expression driven by a nestin gene promoter, respectively. KCNMA1<sup>fl/fl</sup> mice were generated as described (39) and used after back-crossing for six generations. Nestin-Cre mice (61) were obtained from The Jackson Laboratory as the strain of B6.Cg-Tg(Nes-cre)1Kln/J and genotyped as nestin-Cre<sup>+</sup> (homozygous or heterozygous) after cross-breeding. All animal experiments were carried out according to protocols and guidelines approved by the Institutional Animal Care and Use Committee of The University of Texas MD Anderson Cancer Center.

#### Heterologous Expression of BK Channels and NMDARs in Cultured Cells.

Recombinant cDNA constructs of human BK $\alpha$  and the rat glutamate receptor subunits GluN1, GluN2A, GluN2B, GluR1, GluR2, GluK1, and GluK2 were used for heterologous expression in HEK-293 cells. FLAG-tagged GluN1 and V5-tagged BK $\alpha$  were constructed by using a pCDNA6 vector (Invitrogen). Chimeric constructs of GluN1 were obtained from James Huettner, Washington University in St. Louis, St. Louis, MO (36, 37). HEK-293 cells were obtained from ATCC. The cells were transiently transfected with the designated plasmids with Lipofectamine 2000 (Invitrogen) and used for experiments within 16–48 h after transfection.

#### Protein Purification/Precipitation, Mass Spectrometry, and Immunoblotting.

Immunopurification/precipitation of channel proteins from rat brains and cultured cells were carried out essentially as we described (16, 59). Rat brain cell membranes were prepared from freshly isolated adult whole rat brains via tissue homogenization and differential centrifugation at 2,000  $\times$  *g* for 10 min to collect supernatants and then at 100,000  $\times$  *g* for 30 min to collect cell membranes. NMDARs and BK channels were solubilized from rat brain membranes or HEK-293 cells by using 2% dodecyl maltoside in a TBS buffer containing 150 mM NaCl and 20 mM Tris-HCl (pH 8.0). The solubilized membrane proteins were collected as supernatants after centrifugation at 17,000  $\times$  *g* for 10 min and then incubated with an immobilized antibody (1–10 mg) that was covalently cross-linked to protein-A agarose beads. After repetitive washing, the captured proteins were eluted from immunobeads by using 2 $\times$  Laemmli SDS/PAGE sample buffer (4% SDS, 20% glycerol, 0.001% bromophenol blue, 100 mM DTT, and 125 mM Tris-HCl, pH 6.8) or a FLAG peptide (100 mg/mL) for purification made with an anti-FLAG antibody only. The eluted proteins were separated on an SDS/PAGE gel with a complete run for immunoblot analysis or a brief run to collect all proteins in one or two gel bands for mass spectrometric analysis. In-gel digestion and mass spectrometric analysis of purified proteins were performed as described (16, 59), except that a more advanced mass spectrometer, the Orbitrap Fusion Lumos Tribrid (Thermo Scientific), was used for liquid chromatography-tandem mass spectrometric analysis in the present study. To analyze the role of the BK $\alpha$  50–51 loop region (residues 46–93) in BK $\alpha$ –GluN1 interactions, a biotinylated BK $\alpha$ 46–93 peptide (biotin-LKYLWTVWCCHCGGKTKAEQKINNGSSQADGTLKPVDEKEAVAAEVGW-amide) and a scrambled peptide of the same amino acid composition (biotin-GENPDGLWKEKVKIQCKVGAEEATCAHSAGLTVWSNEKDVTCCKLA-amide) were custom-synthesized (Synpeptide Co.). For immunoprecipitation experiments on the ability of the peptide in competition with BK $\alpha$  on interactions with GluN1, the peptides were added to cell lysates at a final concentration of 1 mg/mL and incubated overnight. For in vitro assay of the direct interactions between BK $\alpha$ 46–93 peptide and GluN1's cytosolic regions, the GluN1's two cytosolic regions, M1–M2 loop (residues 563–587) and C terminus (813–920), were expressed in *E. coli* BL21 (DE3) strain as a 6 $\times$  His-tagged fusion protein and purified from the water soluble fraction of cell lysates using nickel-nitrilotriacetic acid (Ni-NTA) column. The purified fusion protein, GluN<sup>cytosolic</sup>, was then incubated with the biotinylated BK $\alpha$ 46–93 and scrambled peptides that were immobilized to the Strep-Tactin agarose beads (IBA Lifesciences) for 4 h, washed three times with TBS, and eluted from beads with Laemmli SDS/PAGE sample buffer. For immunoblot analysis, proteins were electrically transferred from an SDS/PAGE gel to PVDF membranes and then probed with antibodies specifically recognizing the targeted proteins. Rabbit polyclonal anti-GluN1 (catalog no. G8913; Sigma-Aldrich), anti-BK $\alpha$  (catalog no. APC-107; Alomone Labs), anti-GluN2A (catalog no. AB1555; EMD Millipore), anti-GluN2B (catalog no. SAB2104208; Sigma-Aldrich), and anti-FLAG (catalog no. F7425; Sigma-Aldrich) and mouse monoclonal anti-BK $\alpha$  (catalog no. L6/60; NeuroMabs) antibodies were used for immunopurification. For immunoblot analysis, mouse monoclonal anti-GluR1 and -GluR2 (catalog nos. N355/1 and L21/32, respectively; NeuroMab), anti-V5 (catalog no. 46-0709; Invitrogen), anti-Myc

(catalog no. M4436; Sigma-Aldrich), and rabbit polyclonal anti-GFP (catalog no. G1544; Sigma-Aldrich) antibodies were used as well.

**In Situ PLA.** HEK-293 cells were fixed in 4% paraformaldehyde 16–24 h after transfection. Cells with or without permeabilization treatment (0.05% Triton X-100) were incubated with primary antibodies of mouse monoclonal anti-BK $\alpha$  (1:100; catalog no. L6/60; NeuroMab) and rabbit anti-GluN1 (1:200; catalog no. AB9864R; EMD Millipore), or mouse monoclonal anti-V5 (1:500; catalog no. R960-25; Invitrogen) and rabbit anti-FLAG (1:500; catalog no. F7425; Sigma-Aldrich) in phosphate-buffered saline (PBS) at room temperature for 1 h. For brain tissue analysis, 4- to 8-wk-old mice were anesthetized and perfused intracardially with buffered 4% paraformaldehyde in PBS. Brains were removed and postfixed for 2 h in the same paraformaldehyde solution at 4 °C. Fixed brain tissues were incubated first in a 15% and then in a 30% sucrose PBS solution overnight at 4 °C and then cryosectioned at 10–12  $\mu$ m. Brain tissue sections were incubated at 4 °C overnight with primary mouse monoclonal anti-BK $\alpha$  (1:100; NeuroMab) and rabbit anti-GluN1 (1:100; EMD Millipore) antibodies. In situ PLA was performed by using Duolink In Situ PLA reagents (Sigma-Aldrich). HEK-293 cells or brain slices that were already probed with primary antibodies were first incubated with secondary anti-mouse and -rabbit antibodies conjugated with oligonucleotides of a PLA probe and then subjected to oligonucleotide hybridization, ligation, amplification, and detection following the manufacturer's instructions. Finally, cells and brain slices were mounted on slides by using a mounting medium with DAPI and observed under a confocal microscope (catalog no. FV1000; Olympus).

**Electrophysiology.** Hippocampal slices (320  $\mu$ m) were prepared from 4- to 8-wk-old mice by using a vibratome (Leica Biosystems) and kept at room temperature for at least 1 h in artificial cerebral spinal fluid (ACSF) containing 124 mM NaCl, 5 mM KCl, 1.25 mM Na<sub>2</sub>HPO<sub>4</sub>, 2 mM MgSO<sub>4</sub>, 2 mM CaCl<sub>2</sub>, 26 mM NaHCO<sub>3</sub>, and 10 mM D-glucose aerated with 95% O<sub>2</sub> and 5% CO<sub>2</sub>. The hippocampal dentate gyrus was visualized under an infrared differential interference contrast optics microscope (Zeiss). Whole-cell patch-clamp recordings were performed on granule cells with a MultiClamp 700B amplifier (Axon Instruments) at 31–33 °C. Pipette electrodes (3–5 M $\Omega$ ) were filled with 125 mM KMeSO<sub>3</sub>, 4 mM KCl, 10 mM phosphocreatine, 3 mM Mg-ATP, 0.5 mM Na-GTP, 0.2 mM EGTA, and 10 mM Hepes (pH 7.2). In some experiments, 0.2 mM EGTA was replaced with 2 mM EGTA or BAPTA. Only granule cells with a resting membrane potential less than or equal to –80 mV, a characteristic of mature cells (62), and a stable series resistance or capacitance were used for data recording. All experiments were performed in the presence of picrotoxin (100  $\mu$ M) to reduce GABAergic contributions. For recording of glutamate-induced NMDAR and BK channel currents, 6-cyano-7-nitroquinoxaline-2,3-dione (CNQX) at a concentration of 20  $\mu$ M or 6,7-dinitroquinoxaline-2,3-dione (DNQX) at a concentration of 10  $\mu$ M was included in the bath solution to eliminate the fast AMPA receptor currents. Glutamate (100  $\mu$ M) and glycine (10  $\mu$ M) were applied locally to granule cells for 100 ms via a puffer pipette by using a pressurized perfusion system (ALA Scientific Instruments). For measurement of evoked EPSPs and EPSCs, whole-cell current- or voltage-clamp recording was performed on granule cells, and a bipolar stimulating electrode was placed in the middle region of the molecular layer of the dentate gyrus to stimulate the MPP by using a Master-9 pulse stimulator (A.M.P.I.). Subthreshold EPSPs were evoked at 0.05 Hz, and the data collected over a period of 5 min were averaged. For paired-pulse ratio recording, pipettes electrodes were filled with 145 mM K-gluconate, 5 mM NaCl, 1 mM MgCl<sub>2</sub>, 0.2 mM EGTA, 2 mM Mg-ATP, 0.1 mM Na-GTP, and 10 mM Hepes (pH 7.2). Test responses were elicited at 0.03 Hz, and four traces of EPSCs were averaged. All data are expressed as means  $\pm$  SEM. A paired *t* test was used to perform statistical analysis. *P* values < 0.05 were considered significant. Paxil-line, IbTX, CNQX, and DNQX (Alomone Labs), and picrotoxin and MK-801 (Tocris Bioscience) were dissolved in dimethyl sulfoxide, and AP5 (DL-AP-5; Abcam) was dissolved in water to create stock solutions and finally diluted with ACSF to specific concentrations before each experiment. Drugs were applied for 5–10 min before data collection.

**Data Availability.** All data generated or analyzed during this study are included in the main text and [SI Appendix](#).

**ACKNOWLEDGMENTS.** We thank Dr. James Huettner (Washington University in St. Louis) for kind gifts of the GluN1/GluK2 chimeric mutant constructs. Mass spectrometry raw data were collected at the UT Southwestern Proteomic Core. This work was supported by National Institutes of Health Grants NS078152 (to J.Y.), GM127332 (to J.Y.), and HL102758 (to A.L.M.).

- Ghatta S, Nimmagadda D, Xu X, O'Rourke ST (2006) Large-conductance, calcium-activated potassium channels: Structural and functional implications. *Pharmacol Ther* 110:103–116.
- Salkoff L, Butler A, Ferreira G, Santi C, Wei A (2006) High-conductance potassium channels of the SLO family. *Nat Rev Neurosci* 7:921–931.
- Shao LR, Halvorsrud R, Borg-Graham L, Storm JF (1999) The role of BK-type  $\text{Ca}^{2+}$ -dependent  $\text{K}^{+}$  channels in spike broadening during repetitive firing in rat hippocampal pyramidal cells. *J Physiol* 521:135–146.
- Raffaelli G, Saviane C, Mohajerani MH, Pedarzani P, Cherubini E (2004) BK potassium channels control transmitter release at CA3-CA3 synapses in the rat hippocampus. *J Physiol* 557:147–157.
- Hu H, et al. (2001) Presynaptic  $\text{Ca}^{2+}$ -activated  $\text{K}^{+}$  channels in glutamatergic hippocampal terminals and their role in spike repolarization and regulation of transmitter release. *J Neurosci* 21:9585–9597.
- Sausbier M, et al. (2004) Cerebellar ataxia and Purkinje cell dysfunction caused by  $\text{Ca}^{2+}$ -activated  $\text{K}^{+}$  channels in spike broadening during repetitive firing in rat hippocampal pyramidal cells. *Proc Natl Acad Sci USA* 101:9474–9478.
- Meredith AL, et al. (2006) BK calcium-activated potassium channels regulate circadian behavioral rhythms and pacemaker output. *Nat Neurosci* 9:1041–1049.
- Fettiplace R, Fuchs PA (1999) Mechanisms of hair cell tuning. *Annu Rev Physiol* 61:809–834.
- Du W, et al. (2005) Calcium-sensitive potassium channelopathy in human epilepsy and paroxysmal movement disorder. *Nat Genet* 37:733–738.
- Brenner R, et al. (2005) BK channel beta4 subunit reduces dentate gyrus excitability and protects against temporal lobe seizures. *Nat Neurosci* 8:1752–1759.
- Brenner R, et al. (2000) Vasoregulation by the beta1 subunit of the calcium-activated potassium channel. *Nature* 407:870–876.
- Meredith AL, Thorneloe KS, Werner ME, Nelson MT, Aldrich RW (2004) Overactive bladder and incontinence in the absence of the BK large conductance  $\text{Ca}^{2+}$ -activated  $\text{K}^{+}$  channel. *J Biol Chem* 279:36746–36752.
- Werner ME, Zvara P, Meredith AL, Aldrich RW, Nelson MT (2005) Erectile dysfunction in mice lacking the large-conductance calcium-activated potassium (BK) channel. *J Physiol* 567:545–556.
- Yang C, et al. (2017) Knockout of the LRRC26 subunit reveals a primary role of LRRC26-containing BK channels in secretory epithelial cells. *Proc Natl Acad Sci USA* 114:E3739–E3747.
- Li Q, Yan J (2016) Modulation of BK channel function by auxiliary beta and gamma subunits. *Int Rev Neurobiol* 128:51–90.
- Yan J, Aldrich RW (2010) LRRC26 auxiliary protein allows BK channel activation at resting voltage without calcium. *Nature* 466:513–516.
- Yan J, Aldrich RW (2012) BK potassium channel modulation by leucine-rich repeat-containing proteins. *Proc Natl Acad Sci USA* 109:7917–7922.
- Rothberg BS, Magleby KL (1999) Gating kinetics of single large-conductance  $\text{Ca}^{2+}$ -activated  $\text{K}^{+}$  channels in high  $\text{Ca}^{2+}$  suggest a two-tiered allosteric gating mechanism. *J Gen Physiol* 114:93–124.
- Eggermann E, Bucurenciu I, Goswami SP, Jonas P (2011) Nanodomain coupling between  $\text{Ca}^{2+}$  channels and sensors of exocytosis at fast mammalian synapses. *Nat Rev Neurosci* 13:7–21.
- Tay LH, et al. (2012) Nanodomain  $\text{Ca}^{2+}$  of  $\text{Ca}^{2+}$  channels detected by a tethered genetically encoded  $\text{Ca}^{2+}$  sensor. *Nat Commun* 3:778.
- Berkefeld H, et al. (2006)  $\text{BK}_{\text{Ca}}$ -Cav channel complexes mediate rapid and localized  $\text{Ca}^{2+}$ -activated  $\text{K}^{+}$  signaling. *Science* 314:615–620.
- Fakler B, Adelman JP (2008) Control of  $\text{K}_{\text{Ca}}$  channels by calcium nano/microdomains. *Neuron* 59:873–881.
- Marrion NV, Tavalin SJ (1998) Selective activation of  $\text{Ca}^{2+}$ -activated  $\text{K}^{+}$  channels by colocalized  $\text{Ca}^{2+}$  channels in hippocampal neurons. *Nature* 395:900–905.
- Wang K, Lin MT, Adelman JP, Maylie J (2014) Distinct  $\text{Ca}^{2+}$  sources in dendritic spines of hippocampal CA1 neurons couple to SK and Kv4 channels. *Neuron* 81:379–387.
- Ngo-Anh TJ, et al. (2005) SK channels and NMDA receptors form a  $\text{Ca}^{2+}$ -mediated feedback loop in dendritic spines. *Nat Neurosci* 8:642–649.
- Berkefeld H, Fakler B (2008) Repolarizing responses of  $\text{BK}_{\text{Ca}}$ -Cav complexes are distinctly shaped by their Cav subunits. *J Neurosci* 28:8238–8245.
- Prakriya M, Lingle CJ (2000) Activation of BK channels in rat chromaffin cells requires summation of  $\text{Ca}^{2+}$  influx from multiple  $\text{Ca}^{2+}$  channels. *J Neurophysiol* 84:1123–1135.
- Edgerton JR, Reinhart PH (2003) Distinct contributions of small and large conductance  $\text{Ca}^{2+}$ -activated  $\text{K}^{+}$  channels to rat Purkinje neuron function. *J Physiol* 548:53–69.
- Robitaille R, Garcia ML, Kaczorowski GJ, Charlton MP (1993) Functional colocalization of calcium and calcium-gated potassium channels in control of transmitter release. *Neuron* 11:645–655.
- Gola M, Crest M (1993) Colocalization of active  $\text{K}_{\text{Ca}}$  channels and  $\text{Ca}^{2+}$  channels within  $\text{Ca}^{2+}$  domains in helix neurons. *Neuron* 10:689–699.
- Sun X, Gu XQ, Haddad GG (2003) Calcium influx via L- and N-type calcium channels activates a transient large-conductance  $\text{Ca}^{2+}$ -activated  $\text{K}^{+}$  current in mouse neocortical pyramidal neurons. *J Neurosci* 23:3639–3648.
- Isaacson JS, Murphy GJ (2001) Glutamate-mediated extrasynaptic inhibition: Direct coupling of NMDA receptors to  $\text{Ca}^{2+}$ -activated  $\text{K}^{+}$  channels. *Neuron* 31:1027–1034.
- Paoletti P, Bellone C, Zhou Q (2013) NMDA receptor subunit diversity: Impact on receptor properties, synaptic plasticity and disease. *Nat Rev Neurosci* 14:383–400.
- Hite RK, Tao X, MacKinnon R (2017) Structural basis for gating the high-conductance  $\text{Ca}^{2+}$ -activated  $\text{K}^{+}$  channel. *Nature* 541:52–57.
- Tao X, Hite RK, MacKinnon R (2017) Cryo-EM structure of the open high-conductance  $\text{Ca}^{2+}$ -activated  $\text{K}^{+}$  channel. *Nature* 541:46–51.
- Wilding TJ, Lopez MN, Huettner JE (2014) Radial symmetry in a chimeric glutamate receptor pore. *Nat Commun* 5:3349.
- Wilding TJ, Lopez MN, Huettner JE (2016) Chimeric glutamate receptor subunits reveal the transmembrane domain is sufficient for NMDA receptor pore properties but some positive allosteric modulators require additional domains. *J Neurosci* 36:8815–8825.
- Söderberg O, et al. (2006) Direct observation of individual endogenous protein complexes in situ by proximity ligation. *Nat Methods* 3:995–1000.
- Zemen BG, et al. (2015) Generation of Kcnma1fl-tdTomato, a conditional deletion of the BK channel  $\alpha$  subunit in mouse. *Physiol Rep* 3:e12612.
- Zhou Y, Lingle CJ (2014) Paxilline inhibits BK channels by an almost exclusively closed-channel block mechanism. *J Gen Physiol* 144:415–440.
- Carter BC, Jahr CE (2016) Postsynaptic, not presynaptic NMDA receptors are required for spike-timing-dependent LTD induction. *Nat Neurosci* 19:1218–1224.
- Nabavi S, et al. (2013) Metabotropic NMDA receptor function is required for NMDA receptor-dependent long-term depression. *Proc Natl Acad Sci USA* 110:4027–4032.
- Huettner JE, Bean BP (1988) Block of N-methyl-D-aspartate-activated current by the anticonvulsant MK-801: Selective binding to open channels. *Proc Natl Acad Sci USA* 85:1307–1311.
- Corlew R, Wang Y, Ghermazian H, Erisir A, Philpot BD (2007) Developmental switch in the contribution of presynaptic and postsynaptic NMDA receptors to long-term depression. *J Neurosci* 27:9835–9845.
- Smith SL, Smith IT, Branco T, Häusser M (2013) Dendritic spikes enhance stimulus selectivity in cortical neurons in vivo. *Nature* 503:115–120.
- Li Q, Madison R, Moore SD (2014) Presynaptic BK channels modulate ethanol-induced enhancement of GABAergic transmission in the rat central amygdala nucleus. *J Neurosci* 34:13714–13724.
- Furukawa N, Takasusuki T, Fukushima T, Hori Y (2008) Presynaptic large-conductance calcium-activated potassium channels control synaptic transmission in the superficial dorsal horn of the mouse. *Neurosci Lett* 444:79–82.
- Martire M, et al. (2010) Pre-synaptic BK channels selectively control glutamate versus GABA release from cortical and hippocampal nerve terminals. *J Neurochem* 115:411–422.
- Colino A, Malenka RC (1993) Mechanisms underlying induction of long-term potentiation in rat medial and lateral perforant paths in vitro. *J Neurophysiol* 69:1150–1159.
- Cho MH, Cao X, Wang D, Tsien JZ (2007) Dentate gyrus-specific manipulation of beta-Ca2+/calmodulin-dependent kinase II disrupts memory consolidation. *Proc Natl Acad Sci USA* 104:16317–16322.
- Dobrunz LE, Stevens CF (1997) Heterogeneity of release probability, facilitation, and depletion at central synapses. *Neuron* 18:995–1008.
- Sailer CA, et al. (2006) Immunolocalization of BK channels in hippocampal pyramidal neurons. *Eur J Neurosci* 24:442–454.
- Wu ZZ, Li DP, Chen SR, Pan HL (2009) Aminopyridines potentiate synaptic and neuromuscular transmission by targeting the voltage-activated calcium channel beta subunit. *J Biol Chem* 284:36453–36461.
- Matthews EA, Disterhoft JF (2009) Blocking the BK channel impedes acquisition of trace eyeblink conditioning. *Learn Mem* 16:106–109.
- Typlt M, et al. (2013) Mice with deficient BK channel function show impaired prepulse inhibition and spatial learning, but normal working and spatial reference memory. *PLoS One* 8:e81270.
- Springer SJ, Burkett BJ, Schrader LA (2015) Modulation of BK channels contributes to activity-dependent increase of excitability through MTORC1 activity in CA1 pyramidal cells of mouse hippocampus. *Front Cell Neurosci* 8:451.
- Ye H, Jalini S, Mylvaganam S, Carlen P (2010) Activation of large-conductance  $\text{Ca}^{2+}$ -activated  $\text{K}^{+}$  channels depresses basal synaptic transmission in the hippocampal CA1 area in APP (swe/ind) TgCRND8 mice. *Neurobiol Aging* 31:591–604.
- Song B, Marvizi JC (2005) N-methyl-D-aspartate receptors and large conductance calcium-sensitive potassium channels inhibit the release of opioid peptides that induce mu-opioid receptor internalization in the rat spinal cord. *Neuroscience* 136:549–562.
- He S, Wang YX, Petralia RS, Brenowitz SD (2014) Cholinergic modulation of large-conductance calcium-activated potassium channels regulates synaptic strength and spine calcium in cartwheel cells of the dorsal cochlear nucleus. *J Neurosci* 34:5261–5272.
- Griguoli M, Sgritta M, Cherubini E (2016) Presynaptic BK channels control transmitter release: Physiological relevance and potential therapeutic implications. *J Physiol* 594:3489–3500.
- Tronche F, et al. (1999) Disruption of the glucocorticoid receptor gene in the nervous system results in reduced anxiety. *Nat Genet* 23:99–103.
- Lopez-Rojas J, Kreutz MR (2016) Mature granule cells of the dentate gyrus—Passive bystanders or principal performers in hippocampal function? *Neurosci Biobehav Rev* 64:167–174.